Inorganic Chemistry

Article

pubs.acs.org/IC

Control of the Charge Distribution and Modulation of the Class II–III Transition in Weakly Coupled Mo_2–Mo_2 Systems

Xuan Xiao,[†] Chun Y. Liu,*[,†,‡] Qiao He,[§] Mei Juan Han,[†] Miao Meng,[‡] Hao Lei,[‡] and Xin Lu*[,§]

[†]Department of Chemistry, Tongji University, 1239 Siping Road, Shanghai 200092, China

[‡]Department of Chemistry, Jinan University, 601 Huang-Pu Avenue West, Guangzhou 510632, China

[§]State Key Laboratory of Physical Chemistry of Solid Surfaces and Fujian Provincial Key Laboratory of Theoretical and Computational Chemistry, Department of Chemistry, College of Chemistry and Chemical Engineering, Xiamen University, Xiamen 361005, China

Supporting Information

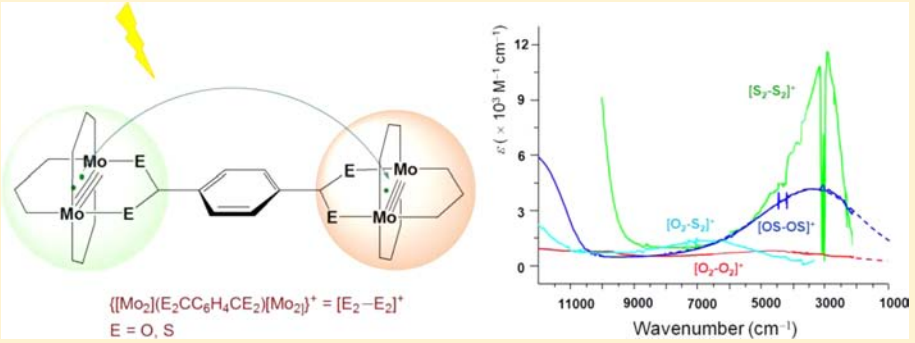

ABSTRACT: Three novel dimolybdenum dimers $[Mo_2(DAniF)_3]_2(\mu\text{-}OSCC_6H_4CSO)$, $[Mo_2(DAniF)_3]_2(\mu\text{-}O_2CC_6H_4CS_2)$, and $[Mo_2(DAniF)_3]_2(\mu\text{-}S_2CC_6H_4CS_2)$ (DAniF = *N*,*N*′-di(*p*-anisyl)formamidinate) have been synthesized and characterized by single-crystal X-ray diffractions. Together with the terephthalate analogue, the four compounds, denoted as $[\mathbf{O_2{-}O_2}]$, $[\mathbf{OS{-}OS}]$, $[\mathbf{S_2{-}S_2}]$, and $[\mathbf{O_2{-}S_2}]$, have similar molecular skeletons and $Mo_2\cdots Mo_2$ separations (~12 Å), but varying sulfur contents or symmetry. The singly oxidized complexes $[\mathbf{O_2{-}O_2}]^+$, $[\mathbf{OS{-}OS}]^+$, $[\mathbf{S_2{-}S_2}]^+$, and $[\mathbf{O_2{-}S_2}]^+$ display characteristic intervalence transition absorption bands in the near- and mid-IR regions, with differing band energy, intensity, and shape. Applying the geometrical length of the bridging group "$-CC_6H_4C-$" (5.8 Å) as the effective electron transfer distance, calculations from the Mulliken–Hush equation yield electronic coupling matrix elements (H_{ab}) in the range 600–900 cm^{-1}. Significantly, this series presents a transition from electron localization to "almost-delocalization" as the carboxylate groups of the bridging ligand are successively thiolated. In terms of Robin–Day's scheme, $[\mathbf{S_2{-}S_2}]^+$ is best described as an intermediate between Class II and III, while $[\mathbf{O_2{-}O_2}]^+$ and $[\mathbf{OS{-}OS}]^+$ belong to Class II. It is unusual that the Class II–III transition occurs in such a weakly coupled system (H_{ab} < 1000 cm^{-1}). This is attributed to the d(δ)–p(π) conjugation between the Mo_2 center and bridging ligand. By electrochemical and spectroscopic methods, the internal energy difference for $[\mathbf{O_2{-}S_2}]^+$ is determined to be 2250 ± 80 cm^{-1}, which controls the charge distribution of the cation radical. The experimental results and theoretical analyses illustrate that the unsymmetrical geometry leads to unbalanced electronic configurations and asymmetrical redox and optical behaviors.

INTRODUCTION

For a study of electronic coupling between two sites within a molecule, the mixed-valence (MV) complex $[(NH_3)_5Ru\text{-}(pyrazine)Ru(NH_3)_5]^{5+}$, namely the Creutz–Taube ion, is the prototype.[1] With this initial compound, a diversity of bridged binuclear d^{5-6} metal complexes have been synthesized and investigated.[2] The synthetic strategies for these compounds include variations of the metal nuclearity, the bridging ligands, the ancillary ligands, as well as the coordination modes. By assembling triruthenium building blocks with a bridging ligand, Ru_3–Ru_3 type complexes have been studied by Ito and Kubiak, and have become excellent experimental models for the study of MV compounds and intramolecular electron transfer.[3] Pure organic compounds have also been employed in these research practices since the 1990s, by which the important optical behaviors of MV compounds are elucidated.[4−6] Thereafter, Chisholm's[7] and Cotton's[8] groups developed M_2–M_2 systems (M = Mo and W) to evaluate the extent of electronic interaction between two covalently bonded dimetal units. The great variety of dimetal complexes provides numerous versatile model compounds for the exploration of mixed-valence phenomenon on the interplay between experiment and theory.

Compared with a single metal center, a dimetal unit has a well-defined electronic configuration, e.g., $\sigma^2\pi^4\delta^2$ for quadruply bonded Mo_2 and W_2 units.[9] The formation of metal–metal

Received: July 16, 2013
Published: October 23, 2013

multiple bonds removes the d orbital degeneracy, with two valence electrons residing on the δ orbital. Thus, single electron transfer across the bridge is explicitly due to the behaviors of the δ electrons. When two dimetal units are bridged by a conjugated ligand, the metal−ligand electronic coupling is promoted by the d(δ)−p(π) orbital interaction. Undoubtedly, these unique features of the "dimers of dimers" are greatly beneficial to spectroscopic analysis of the charge transfer and mechanistic study on the electron exchange reactions.

In this article, two symmetrical and one unsymmetrical dimolybdenum dimers have been synthesized by assembling two units of $[Mo_2(DAniF)_3]^+$ with partially and fully thiolated terephthalate bridging ligands, where DAniF is the auxiliary ligand, *N*,*N*′-di(*p*-anisyl)formamidinate. Together with the terephthalate analogue,[10] the family consists of four members, $[Mo_2(DAniF)_3]_2(\mu\text{-}O_2CC_6H_4CO_2)$, $[Mo_2(DAniF)_3]_2(\mu\text{-}OSCC_6H_4CSO)$, $[Mo_2(DAniF)_3]_2(\mu\text{-}S_2CC_6H_4CS_2)$, and $[Mo_2(DAniF)_3]_2(\mu\text{-}O_2CC_6H_4CS_2)$ (Scheme 1), hereafter abbreviated as $[\mathbf{O_2{-}O_2}]$, $[\mathbf{OS{-}OS}]$, $[\mathbf{S_2{-}S_2}]$, and $[\mathbf{O_2{-}S_2}]$. The structures of these four complexes have similar molecular scaffolds as determined by single-crystal X-ray diffractions. Significantly, they share a common mechanism for the electronic coupling and the intramolecular electron transfer because of their isoelectronic valence shells. Single electron oxidation of the four compounds yielded the corresponding mixed-valence radical cations, $[\mathbf{O_2{-}O_2}]^+$, $[\mathbf{OS{-}OS}]^+$, $[\mathbf{S_2{-}S_2}]^+$ and $[\mathbf{O_2{-}S_2}]^+$. In the near-IR to mid-IR spectrum, each of these complexes displayed a characteristic intervalence transition band, by which we were able to estimate the coupling parameter H_{ab} using the Hush model,[11] on the basis of which the extent of electron delocalization for the MV species was assessed in terms of Robin−Day's scheme.[12] More importantly, we explored the gradient impact on electron distribution and Class II to III transition due to the sulfur atoms being successively introduced to the bridging ligand, while other structural and electronic factors remain unchanged. For the unsymmetrical $[\mathbf{O_2{-}S_2}]^+$, there exists an intrinsic potential difference between the donor and acceptor, which controls the charge distribution and intramolecular electron transfer. The values of this parameter (2250 ± 80 cm^{-1}) determined by electrochemical and spectroscopic methods are in remarkable agreement.

Scheme 1[a]

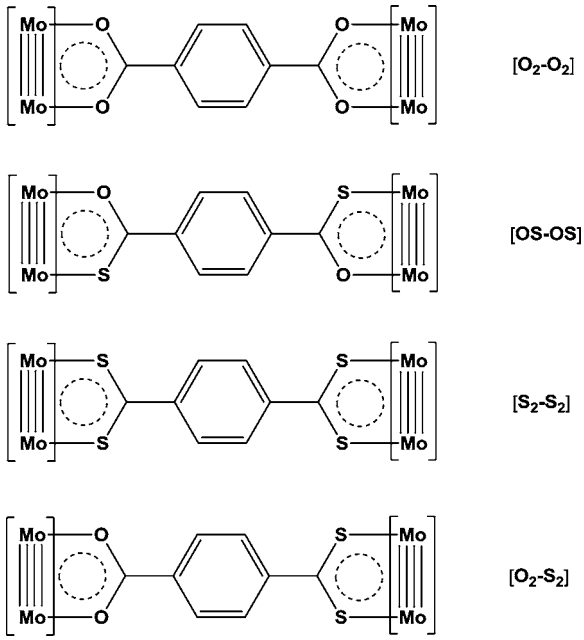

[a] $[Mo_2] = [Mo_2(DAniF)_3]^+$. DAniF = *N*,*N*′-di(*p*-anisyl)formamidinate.

RESULTS AND DISCUSSION

Molecular Design and Synthesis. It is noteworthy that the δ electrons in a quadruply bonded $[Mo_2]$ unit are not confined within the metal−metal bond, but delocalized over the coordination shell through d(δ)−p(π) orbital interactions between the metals and the equatorial chelating groups. Hence, the electron cloud of a dimetal center is relatively loose, and the redox potential of a $[Mo_2]$ unit is very sensitive to variation of the coordination environment.[13] Thus, it is reasonable to consider the $[Mo_2]$ complex unit, rather than the naked Mo_2^{4+} cation, as the electron donor or acceptor. In this study, we chose three different $[Mo_2]$ units $[Mo_2(DAniF)_3(\mu\text{-}O_2C{-})]$, $[Mo_2(DAniF)_3(\mu\text{-}OSC{-})]$, and $[Mo_2(DAniF)_3(\mu\text{-}S_2C{-})]$ as the electron donors, their oxidative counterparts as the corresponding acceptors, and a phenylene group as the common bridge for the D−B−A assemblies (Scheme 1). It is expected that successive increase of sulfur content on the $[Mo_2]$ unit would induce systematical alternation of the electronic properties for the donor and acceptor.

Furthermore, the electron transfer platform in the $Mo_2{-}Mo_2$ system is significantly different from those in the Ru−Ru,[2] $Ru_3{-}Ru_3$,[3] and pure organic systems.[6] When a bridging ligand $(E_2C{-}X{-}CE_2)^{2-}$ (E = O, N, or S) is employed for assembling two dimetal building blocks, the resultant dimer of dimers can be either a conjugated or a nonconjugated system, depending on the nature of the central moiety X. In the current study, the metal to metal electron transfer platform is conjugated and extended to about 17 Å as shown in Scheme 2. The $Mo_2{\cdots}Mo_2$ separation is about 12 Å, as measured between the centroids of the two dimetal units. However, the effective electron transfer distance should be much shorter. As discussed above, electron transfer from the donor to the acceptor crosses the phenylene group; thus, the geometrical length of the "$-CC_6H_4C-$" group, ca. 6 Å, may be considered as the effective electron transfer distance (Scheme 2), in the case where electroabsorption (Stark effect) method[14] for accurate determination of this distance is unavailable.

Scheme 2

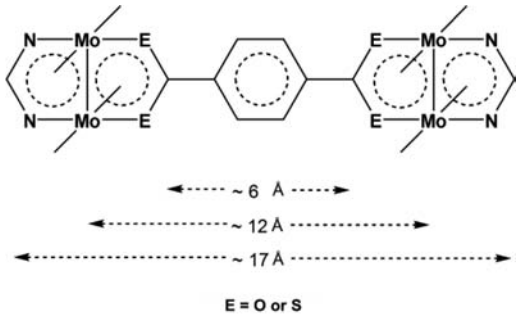

The studied dimers of dimers are assembled by mixing a designed dimolybdenum precursor $Mo_2(DAniF)_3(O_2CCH_3)$ with the bridging ligand at ambient condition, a general procedure developed for preparation of dimolybdenum

dx.doi.org/10.1021/ic4017855 | *Inorg. Chem.* 2013, 52, 12624−12633

Table 1. Crystallographic Data for [OS−OS]·4.5CH_2Cl_2, [S_2−S_2]·2.6CH_2Cl_2·1.5CH_3CH_2OH, and [O_2−S_2]·5CH_2Cl_2

	[OS−OS]	[S_2−S_2]	[O_2−S_2]
formula	$C_{102.5}H_{102}Cl_9Mo_4N_{12}O_{14}S_2$	$C_{103.60}H_{104.10}Cl_{5.20}Mo_4N_{12}O_{13.5}$ S_4	$C_{103}H_{98}Cl_{10}Mo_4N_{12}O_{14}S_2$
Fw	2494.03	2429.63	2530.34
space group	$P\bar{1}$	$P\bar{1}$	$P\bar{1}$
a (Å)	11.3042(6)	10.458(4)	10.1019(6)
b (Å)	14.4059(8)	13.999(5)	13.9079(9)
c (Å)	18.3542(9)	20.600(8)	20.5038(1)
α (deg)	103.699(5)	77.172(5)	77.942(5)
β (deg)	101.997(4)	79.503(5)	76.863(5)
γ (deg)	101.522(5)	74.101(5)	73.901(5)
V (Å^3)	2741.3(2)	2804.4(2)	2662.3(3)
Z	1	1	1
T (K)	150(2)	173(2)	150(2)
d_{calcd} (g/cm^3)	1.510	1.439	1.578
μ (mm^{-1})	6.570	0.698	7.001
R1[a]	0. 0669	0.0561	0.0654
wR2[b]	0. 1740	0.1377	0.1619

[a] $R1 = \Sigma||F_o| - |F_c||/\Sigma|F_o|$. [b] $wR2 = [\Sigma[w(F_o^2 - F_c^2)^2]/\Sigma[w(F_o^2)^2]]^{1/2}$.

Table 2. Selected Bond Distances (Å) of [OS−OS], [S_2−S_2], and [O_2−S_2], in Comparison with Those of [O_2−O_2][a]

				[O_2−S_2]	
	[O_2−O_2]	[OS−OS]	[S_2−S_2]	OO (Mo3Mo4)	SS (Mo1Mo2)
Mo(1)−Mo(2)	2.090(1)	2.1051(6)	2.103(1)	2.097(1)	2.107(2)
Mo(1)−N(1)	2.155(5)	2.133(4)	2.149(5)	2.295(2)	2.094(2)
Mo(1)−N(3)	2.123(5)	2.143(4)	2.153(5)	1.964(2)	2.380(2)
Mo(1)−N(5)	2.152(5)	2.137(4)	2.146(5)	2.105(2)	2.293(2)
Mo(2)−N(2)	2.137(5)	2.161(4)	2.141(5)	2.260(2)	2.078(2)
Mo(2)−N(4)	2.119(5)	2.174(4)	2.164(5)	1.938(2)	2.369(2)
Mo(2)−N(6)	2.137(5)	2.142(4)	2.148(5)	2.079(2)	2.242(2)
Mo(1)−O(7)	2.144(4)	2.112(4)		2.22(3)	
Mo(2)−O(8)	2.122(4)			2.24(3)	
Mo(1)−S(1)			2.442(2)		2.32(2)
Mo(2)−S(2)		2.469 (1)	2.445(2)		2.319(2)
C(4)−C(5)	1.480(2)	1.485(2)	1.487(2)	1.480(2)	1.470(2)
C(4)−S(1)			1.695(6)		1.75(5)
C(4)−S(2)			1.688(6)		1.70(4)
C(4)−O(7)	1.266(7)	1.266(7)		1.52(8)	
C(4)−O(8)	1.279(6)			1.18(8)	
Mo_2···Mo_2	11.24	11.67	12.24	11.79	11.79

[a] Data cited from ref 10a.

compounds of this category.[15] The synthesis and structure for [S_2−S_2] have been reported in a preliminary communication.[16] For the complexes with O/S mixed donors on the bridging ligands, two geometric isomers were obtained, that is, symmetrical [OS−OS] and unsymmetrical [O_2−S_2]. The development of this complete Mo_2−Mo_2 series allows us to systematically examine the influence of subtle structural variation (i.e., different sulfur content and symmetry on the bridging ligand) on the metal−metal coupling interaction.

Molecular Structures. The three dimolybdenum oligomers [OS−OS], [O_2−S_2], and [S_2−S_2] all crystallize in a triclinic $P\bar{1}$ space group with the molecules residing in a special position (Z = 1). The crystallographic data are presented in Table 1, and the selected bond distances, along with corresponding geometrical parameters for the [O_2−O_2] analogue, are listed in Table 2. The structure of [OS−OS] has two identical [Mo_2(DAniF)$_3$(OSC)] units, and the O and S atoms on the bridging ligand are arranged in trans position (Figure 1A). However, the crystal structure of the unsymmetrical [O_2−S_2] is intrinsically disordered. Routine treatments were conducted by separating the dimetal core of the independent unit into two parts. Refinements of the "two halves" of the molecule, [Mo_2(DAniF)$_3$($O_2CCC_3H_2$)] and [Mo_2(DAniF)$_3$($S_2CCC_3H_2$)], with a fixed FVAR (free variable of 0.5) gave satisfactory results. After symmetry generation, the molecular view (Figure 1C) was drawn by combining the two unsymmetrical parts.

Each of the molecules in this family shows a typical Mo−Mo quadruple bond length. In [O_2−S_2], the two different Mo_2 units have the metal−metal bond distances of 2.097(1) and 2.107(2) Å, which are comparable with those found in [O_2−O_2] and [S_2−S_2], respectively. However, the Mo−S bonds are shorter while the Mo−O bonds are longer than those in the related symmetrical analogues (Table 2). One explanation of this is that, in the unsymmetrical molecule, the π electron density is unequally distributed and the d(δ)−p(π) orbital interaction in the thiolated [Mo_2] unit is more efficient than that in the carboxylate dimetal unit. The C(4)−C(5) and C(7)−C(8) bonds in [O_2−S_2], which connect the dimetal unit

dx.doi.org/10.1021/ic4017855 | Inorg. Chem. 2013, 52, 12624−12633

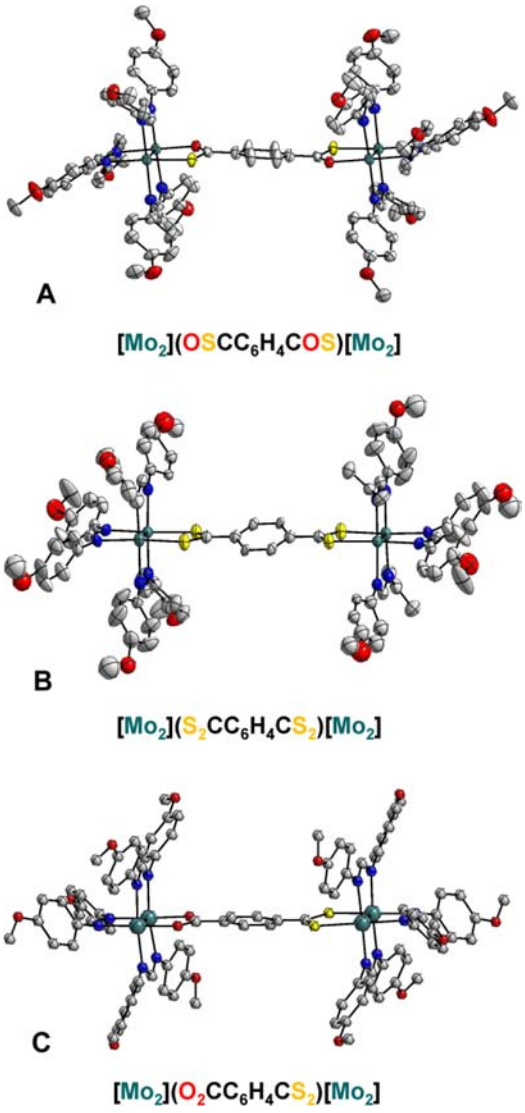

Figure 1. X-ray crystal structures for the dimolybdenum dimers with thiolated teterephthalate bridging ligands. In the compound formulas underneath the structures, $[Mo_2]$ represents the dimetal building block $[Mo_2(DAniF)_3]^+$.

and the phenylene group, are 1.470−1.480 Å in length, appreciably shorter than a normal C−C single bond (ca. 1.52 Å). The decreased C−C bond length is possibly a result of the π orbital interaction between the $[Mo_2]$ unit (δ) and the bridging ligand (π). Finally, in the series, the $Mo_2\cdots Mo_2$ separations vary from 11.24 to 12.24 Å. The thiolated derivatives have the larger metal to metal separations because of the longer Mo−S bonds (Table 2).

Electrochemical Studies. All the four compounds in the series present two successive one-electron redox couples in the electrochemical voltammograms (CV) (Figure 2). Electrochemical oxidations of the Mo_2−Mo_2 complexes in the given potential range remove one δ electron from each of the two bridged Mo_2^{4+} units. In the symmetrical series, the potential separation ($\Delta E_{1/2}$) between the two redox couples increases from 91 mV for $[\mathbf{O_2}-\mathbf{O_2}]$ to 195 mV for $[\mathbf{S_2}-\mathbf{S_2}]$, via 116 mV for the partially thiolated $[\mathbf{OS}-\mathbf{OS}]$ derivative (Table 3). With similar $Mo_2\cdots Mo_2$ distances for these compounds, the observed variation trend in $\Delta E_{1/2}$ indicates that sulfur donors on the bridging ligand greatly enhance the electronic communication

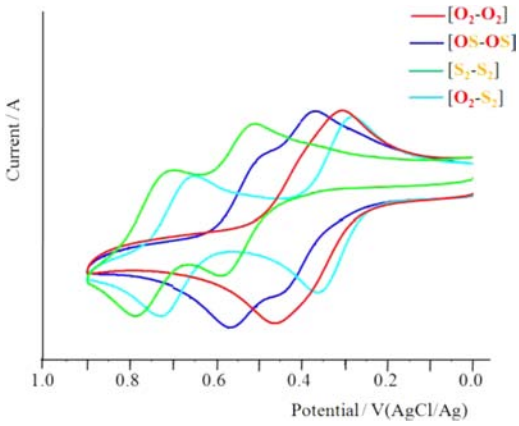

Figure 2. Cyclic voltammograms (CV) for $[\mathbf{O_2}-\mathbf{O_2}]$, $[\mathbf{OS}-\mathbf{OS}]$, $[\mathbf{S_2}-\mathbf{S_2}]$, and $[\mathbf{O_2}-\mathbf{S_2}]$ as labeled in different colors.

Table 3. Electrochemical Measurements and the Parameters for the Comproportionation Equilibriums

compd	$E_{1/2}(1)$ (mV)	$E_{1/2}(2)$ (mV)	$\Delta E_{1/2}$ (mV)	K_c	ΔG_s (cm^{-1})
$[\mathbf{O_2}-\mathbf{O_2}]$	335	426	91	35	−733
$[\mathbf{OS}-\mathbf{OS}]$	468	584	116	91	−935
$[\mathbf{S_2}-\mathbf{S_2}]$	502	697	195	1980	−1572
$[\mathbf{O_2}-\mathbf{S_2}]$	292	652	360	1.2×10^6	−2902

between the two dimetal sites. Given the same auxiliary ligand for the complexes, the redox potentials of a dimetal unit depend mainly on the chelating group from the bridging ligand. For example, removal of the first electron from $[\mathbf{O_2}-\mathbf{O_2}]$ takes place at 335 mV, while this process for $[\mathbf{S_2}-\mathbf{S_2}]$ occurs at 502 mV. Single-electron oxidation of $[\mathbf{O_2}-\mathbf{S_2}]$ shows the redox couple at 292 mV. This indicates that, for the unsymmetrical complex, the electron is removed selectively from the carboxylate associated $[Mo_2]$ unit. Therefore, the electrochemical results support our hypothesis that a coordination saturated $[Mo_2]$ unit serves as the electron donor or acceptor in the MV complexes and the phenylene group ($-C_6H_4-$) functions as the "electron transfer bridge".

The two dithiolated isomers present distinct electrochemical behaviors. The symmetrical $[\mathbf{OS}-\mathbf{OS}]$ has a potential separation reasonably larger than that for $[\mathbf{O_2}-\mathbf{O_2}]$ but smaller than that for $[\mathbf{S_2}-\mathbf{S_2}]$ (Table 3). Its unsymmetrical isomer ($[\mathbf{O_2}-\mathbf{S_2}]$), however, has a notably large $\Delta E_{1/2}$ value (ca. 360 mV). In this case, there is an intrinsic potential difference, namely ΔE_{ip}, between the two different redox sites. An estimation of the ΔE_{ip} value is necessary to determine the degree of electronic communication in $[\mathbf{O_2}-\mathbf{S_2}]$. For this purpose, two reference compounds that resemble the two redox sites in $[\mathbf{O_2}-\mathbf{S_2}]$, $Mo_2(DAniF)_3(O_2CC_6H_5)$ and $Mo_2(DAniF)_3(S_2CC_6H_5)$, were prepared. Their potentials for oxidation $Mo_2^{4+} \rightarrow Mo_2^{5+}$ are measured to be 375 and 651 mV, respectively. Therefore, the potential difference (276 mV) can be an estimate of the internal potential difference (ΔE_{ip}) for $[\mathbf{O_2}-\mathbf{S_2}]$. Now, subtracting this value from the total potential separation $\Delta E_{1/2}$ (ca. 360 mV) gives a "net" potential displacement of 84 mV. Presumably, this is the energetic factor that accounts for electronic coupling between the two dimetal units in $[\mathbf{O_2}-\mathbf{S_2}]$. On this basis, the metal to metal electronic interaction in the unsymmetrical isomer is weaker than that in the symmetrical one, which is convincible.

dx.doi.org/10.1021/ic4017855 | Inorg. Chem. 2013, 52, 12624−12633

Table 4. Calculated Bond Distances and Energy Levels of the Selected Frontier Molecular Orbitals

	bond distances (Å)				orbital energy gap (eV)		MLCT (cm^{-1})	
model	Mo−Mo	$Mo_2\cdots Mo_2$	Mo−O	Mo−S	ΔE_{H-L}[a]	ΔE_{H-H-1}[b]	expt	calcd[c]
$[O_2-O_2]$	2.116	11.320	2.144		2.26	0.13	20 600	18 230
[OS−OS]	2.124	11.769	2.104	2.498	1.90	0.22	16 040	15 330
$[S_2-S_2]$	2.127	12.383		2.466	1.81	0.27	13 850	14 600
$[O_2-S_2]$	2.115	11.845	2.143	2.466	1.71	0.44	15 920	13 960
	2.127							

[a]HOMO−LUMO energy gap. [b]HOMO−HOMO−1 energy gap. [c]The values (cm^{-1}) converted from the ΔE_{H-L} (eV).

The internal potential difference for an unsymmetrical D−B−A system is referred to as the driving force ΔG°, which controls the ET reaction and determines the thermodynamic stability of the ET product. Furthermore, in Marcus−Hush theory,[11b,17] the vertical excitation energy (E_{IT}) for optical electron transfer is a sum of reorganization energy (λ) and free energy change (ΔG°) (eq 1)

$$E_{IT} = \Delta G^\circ + \lambda \quad (1)$$

However, it is usually difficult to verify this energetic relationship experimentally. To determine the intrinsic potential difference in Ru−Os complexes, an approach taken by Meyer was to turn to the structural analogue Ru−Ru dimer.[18] By taking the same approach for the present case, the internal energy difference or ΔG° is estimated from the potential separations, $\Delta E_{1/2}$ for $[\mathbf{O_2-S_2}]$ (360 mV) and $[\mathbf{O_2-O_2}]$ (91 mV)

$$\Delta G^\circ = \Delta(\Delta E_{1/2}) = E_{1/2}([\mathbf{O_2-S_2}]^+) - E_{1/2}([\mathbf{O_2-O_2}]^+) \quad (2)$$

From the electrochemical data (Table 3), the internal potential difference ΔG° for $[\mathbf{O_2-S_2}]^+$ is determined to be 269 mV (or 2170 cm^{-1}). This value is in excellent agreement with 276 mV (or 2230 cm^{-1}) estimated from the two related dimolybdenum monomers.

For this dimetal system, the comproportionation equilibrium can be expressed by

$$[Mo_2-Mo_2]^0 + [Mo_2-Mo_2]^{2+} \rightleftharpoons 2[Mo_2-Mo_2]^+ \quad \Delta G_c$$

where $[Mo_2-Mo_2]^{n+}$ represents the neutral ($n = 0$), mixed-valence ($n = 1$), and doubly oxidized ($n = 2$) complexes. The free energy change (ΔG_c), which measures the thermodynamic stability of the MV complex, is the sum of several energetic factors (eq 3).[2b,19]

$$\Delta G_c = \Delta G_s + \Delta G_e + \Delta G_i + \Delta G_r \quad (3)$$

The comproportionation constant (K_c) is exponentially functional to the redox potential separation $\Delta E_{1/2}$, as described by the expression $K_c = \exp(\Delta E_{1/2}/25.69)$.[20] Accordingly, the magnitude of ΔG_c can be electrochemically determined (Table 3). Of the four terms that contribute to ΔG_c, ΔG_e (electrostatic effect) and ΔG_r (electronic resonance effect) jointly account for the strength of electronic interaction between the two dimetal sites. For the three symmetrical complexes, the differences in ΔG_e should be small and negligible because of the structural similarities. Likewise, the systematic differences between these analogues in statistic (ΔG_s) and inductive factors (ΔG_i) are minimized. Therefore, in this system, the magnitude of ΔG_c reflects the extent of electronic delocalization. The most negative ΔG_c value for the fully thiolated complex (Table 3) demonstrates the great extent of electron delocalization in $[\mathbf{S_2-S_2}]^+$. In contrast, for the unsymmetrical $[\mathbf{O_2-S_2}]$, the large ΔG_c absolute value is due to the internal energy difference, a term that is not present in the symmetrical case. It is necessary to mention that this term makes no contribution to the metal to metal coupling effect, although it has great significance in stabilizing the mixed-valence species. From the large comproportionation constant (1.2×10^6) and small "net" potential displacement (84 mV), the MV species $[\mathbf{O_2-S_2}]^+$ is expected to be thermodynamically more stable and electronically more localized.

Electronic Structures and Spectroscopic Properties. DFT calculations were performed on the basis of the calculation models derived from the molecular structures by replacement of the anisyl groups with hydrogen atoms. The calculated bond distances for the four models, as listed in Table 4, are in good agreement with those found on the X-ray structures. The d(δ)−p(π) orbital interactions between the dimetal units and the bridging ligand can be qualitatively described by Scheme 3. The resultant frontier molecular orbitals, along with the fragment orbitals, are shown in Figure 3. The HOMO results from the out-of-phase ($\delta - \delta$) combination of the δ orbitals with a filled π orbital of the bridging ligand, while the HOMO−1 is obtained by the in-phase ($\delta + \delta$) combination of the δ orbitals with an empty π^* orbital from the ligand. These two occupied metal orbitals are nondegenerate because of the metal−ligand interactions. The magnitude of the energy gap between HOMO and HOMO−1 or ΔE_{H-H-1} signals the strength of the electronic interaction between the two Mo_2 units. The stronger the interaction becomes, the larger the energy gap is. The fully thiolated model has a ΔE_{H-H-1} of 0.27 eV, while this value for the carboxylate analogue is 0.13 eV. The partially thiolated analogue has a ΔE_{H-H-1} value between them (ca. 0.22 eV). We can also evaluate the extent of the

Scheme 3. Diagram for the Orbital Interactions Between the Dimetal Units (d_δ) and the Bridging Ligand (p_π) Which Generate the Frontier Molecular Orbitals

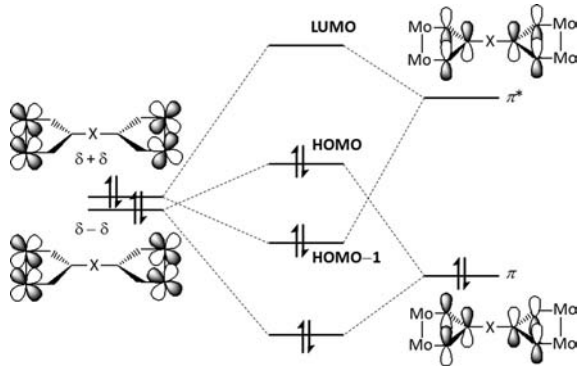

dx.doi.org/10.1021/ic4017855 | Inorg. Chem. 2013, 52, 12624−12633

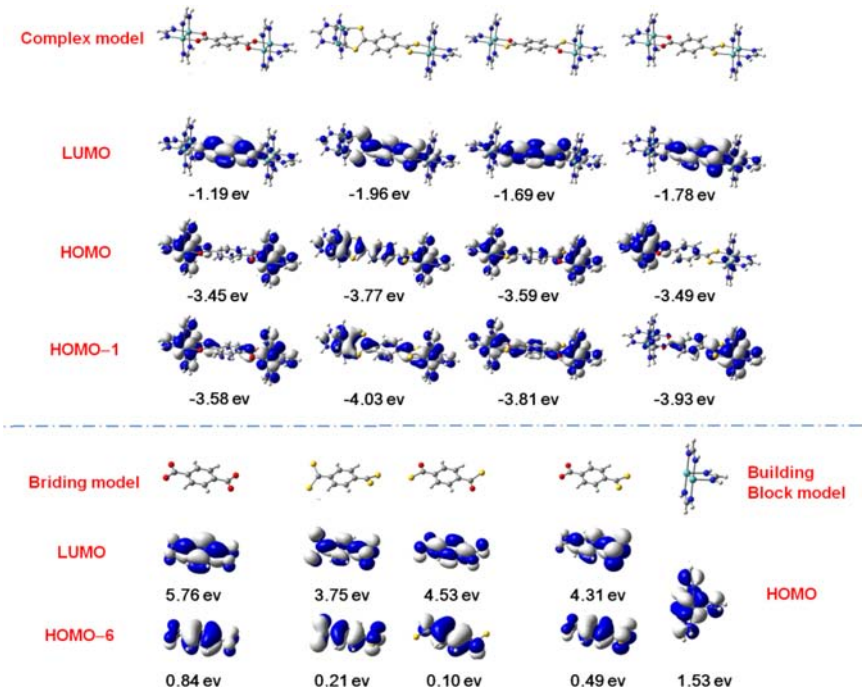

Figure 3. Illustrations of the 0.04 contour surface and energy of the DFT calculated frontier molecular orbitals from models $[Mo_2(N_2H_2CH)_3]_2(E_2CC_6H_4CE_2)$ [E = O (red), S (yellow)] for compounds $[Mo_2(DAniF)_3]_2(E_2CC_6H_4CE_2)$. The orbitals for the fragments are shown below.

metal−ligand interactions by the HOMO−LUMO energy gap, or ΔE_{H-L}. Strong metal−bridging−ligand interaction gives rise to a small HOMO−LUMO gap. The $[\mathbf{S_2}-\mathbf{S_2}]$ model shows the smallest ΔE_{H-L}, ca. 1.81 eV, while the largest energy gap, 2.26 eV, is found for the $[\mathbf{O_2}-\mathbf{O_2}]$ model (Table 4). These calculation results are consistent with the electrochemical analyses, showing a steady increase of the metal to metal interaction as the content of sulfur on the bridging ligand increases. The role of sulfur donor atoms in enhancing the electronic coupling is recognized by several groups,[15b,16,21] which is manifested through this series. As shown in Figure 3, tetrathioterephthalate provides a low energy π^* orbital to react with the in-phase metal orbitals ($\delta + \delta$), generating low energy LUMO and HOMO−1. Thus, the model of $[\mathbf{S_2}-\mathbf{S_2}]$ has a large ΔE_{H-H-1} but a small ΔE_{H-L}.

However, the correlations established between the extent of electronic interactions and the orbital energy gaps are not applicable for the unsymmetrical species, although the same orbital combining regulations are adopted for the formation of the MOs. Calculations on the $[\mathbf{O_2}-\mathbf{S_2}]$ model produce a small ΔE_{H-L} (1.71 eV) but a large ΔE_{H-H-1} (0.44 eV). As shown in Figure 3, the orbital interactions of the dimetal units with the unsymmetrical bridging ligand generate electronically unbalanced MOs. The HOMO is concentrated on the carboxylate supported Mo_2 site, while the HOMO−1 has a condensed electron density on the other site. Similar results have been reported recently in another unsymmetrical Mo_2-Mo_2 system.[22] In the previous section, it is pointed out that the potential separation ($\Delta E_{1/2}$) for $[\mathbf{O_2}-\mathbf{S_2}]$ does not reflect the degree of the electronic coupling between the two dimetal sites. Likewise, the orbital energy gaps ΔE_{H-L} and ΔE_{H-H-1} cannot be used to gauge the strength of the metal−metal and metal−ligand interactions, respectively.

As is well-known, for dimolybdenum (Mo_2^{4+}) paddlewheel compounds, the characteristic absorbance is due to the $\delta \rightarrow \delta^*$ transition occurring in a relatively high energy region (400−500 nm). For these "dimers of dimers", as shown in Figure 4, this

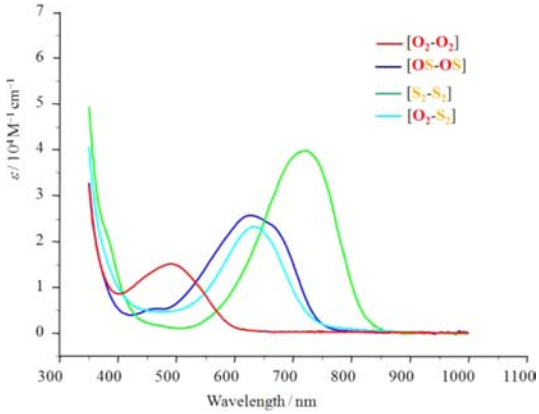

Figure 4. Electronic spectra of the neutral complexes.

band is either invisible or weakened as seen for $[\mathbf{OS}-\mathbf{OS}]$. In the spectra, each of the complexes displays an intense absorption band in the visible region. The band energy decreases, but the intensity increases as the bridging ligand is stepwise thiolated (Figure 4). A high energy band (λ_{max} 492 nm) is found for $[\mathbf{O_2}-\mathbf{O_2}]$ and a low energy band (λ_{max} 715 nm) for $[\mathbf{S_2}-\mathbf{S_2}]$. The absorbencies for the two dithiolated complexes $[\mathbf{OS}-\mathbf{OS}]$ and $[\mathbf{O_2}-\mathbf{S_2}]$ are similar in band energy and intensity, ca. 637 nm (ε, 2.6×10^4 M^{-1} cm^{-1}) for $[\mathbf{O_2}-\mathbf{S_2}]$ and 618 nm (ε, 2.3×10^4 M^{-1} cm^{-1}) for $[\mathbf{OS}-\mathbf{OS}]$. The band energies are comparable with the DFT calculated energies for the HOMO to LUMO transitions (Table 4). Therefore, these bands are ascribable to the HOMO → LUMO excitation, or metal to ligand charge transfer (MLCT).

dx.doi.org/10.1021/ic4017855 | Inorg. Chem. 2013, 52, 12624−12633

Magnetic and Optical Behaviors of the Mixed-Valence Complexes. The MV cation radicals, $[O_2{-}O_2]^+$, $[OS{-}OS]^+$, $[S_2{-}S_2]^+$, and $[O_2{-}S_2]^+$, were prepared by one-electron oxidation of the corresponding neutral molecules using 1 equiv of ferrocenium hexafluorophosphate (Cp_2FePF_6) in CH_2Cl_2 solution. In the X-band electron paramagnetic resonance (EPR) spectra, each complex cation shows one peak having some hyperfine structure (Figure 5). The main

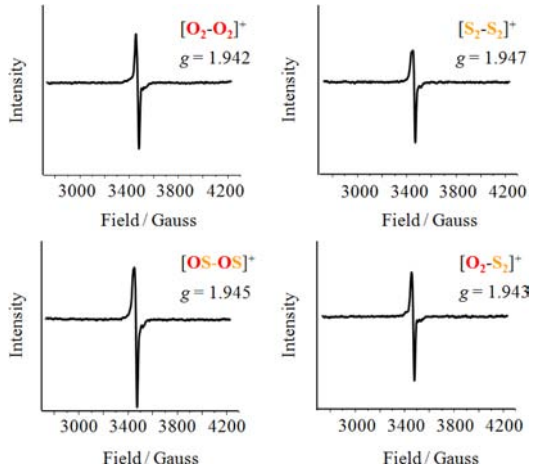

Figure 5. X-band EPR spectra of the radical cations generated by single oxidation of the neutral compounds. Samples were measured in CH_2Cl_2 solutions at 173 K.

EPR signal is attributed to molecules containing only the ^{96}Mo (I = 0) isotope, while the hyperfine structure is due to molecules with one ^{95,97}Mo ($I = {}^5/_2$) isotope, which has a natural abundance of about 25%. Importantly, the g values with varying range from 1.942 to 1.947 are smaller than the value expected for a free organic radical (ca. 2.003), indicating unambiguously that the odd electron resides in a metal-based orbital. The g value for $[O_2{-}O_2]^+$ is 1.942, and for $[S_2{-}S_2]^+$, 1.947, exactly the same as that for a strongly coupled $[Mo_2{-}Mo_2]^+$ cation.[23] For this series, the g values tend to increase as a result of increasing sulfur content, although the variation is small. It appears that the g value is correlated to the extent of electron delocalization. For the two partially thiolated isomers, the unsymmetrical complex $[O_2{-}S_2]^+$ has a g value of 1.943, smaller than 1.945 for $[OS{-}OS]^+$, as expected.

All the mixed-valence species exhibit a broad absorption band in the near-IR to mid-IR regions (Figure 6 and Table 5), which should be assigned to the metal to metal charge transfer (MMCT) or intervalence transition (IT). The band characteristics such as energy, intensity, and shape vary significantly, despite the subtle differences between the compounds. For example, the fully thiolated complex $[S_2{-}S_2]^+$ exhibits a low energy (E_{IT}, 2646 cm^{-1}) and intense (ε_{IT}, 12660 M^{-1} cm^{-1}) IT band. However, the MMCT band for $[O_2{-}O_2]^+$ has much higher energy (E_{IT}, 4240 cm^{-1}) and lower intensity (ε_{IT}, 1470 M^{-1} cm^{-1}). It is interesting to note that, for the three symmetrical species, increasing sulfur content to a higher level lowers the E_{IT} by 800 cm^{-1}. Hereby, the IT band for $[S_2{-}S_2]^+$ is red-shifted by exactly 1600 cm^{-1} relative to that for $[O_2{-}O_2]^+$. The MMCT bands of $[O_2{-}O_2]^+$ and $[OS{-}OS]^+$ are essentially Gaussian-shaped as shown in Figure 6. In contrast, the fully thiolated analogue has an asymmetrical IT band due to the so-called cut-off effect.[4,24] Furthermore, in comparison with

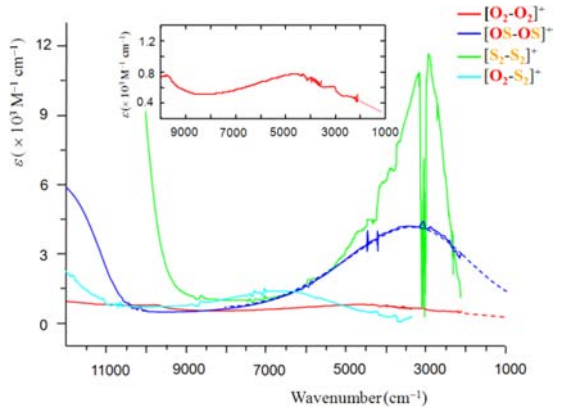

Figure 6. Near- to mid-infrared spectra for the MV complexes, showing the intervalence transitions. For $[O_2{-}O_2]^+$ and $[OS{-}OS]^+$, the IV bands are overlapped in the low energy region with the compacted IR bands from vibrational modes. The spectrum for $[O_2{-}O_2]^+$ is shown in the inset due to the low intensity. The full profiles are generated by simulations with Gaussian-shaped curves (dashed lines).

Table 5. Spectroscopic Data of the IV Bands for the $[O_2{-}O_2]^+$, $[OS{-}OS]^+$, $[S_2{-}S_2]^+$, and $[O_2{-}S_2]^+$ and Electronic Coupling Parameters

compd	E_{IT} (cm^{-1})	ε_{IT} (M^{-1} cm^{-1})	calcd $\Delta\nu_{1/2}$ (cm^{-1})	expt $\Delta\nu_{1/2}$ (cm^{-1})	H_{ab} (cm^{-1})
$[O_2{-}O_2]^+$	4240	1470	3190	4410	560
$[OS{-}OS]^+$	3440	3690	2820	3290	730
$[S_2{-}S_2]^+$	2640	12660	2470	1770	870
$[O_2{-}S_2]^+$	6560	2270	3890	4130	NA

other MV systems, the MMCT absorbencies for this series appear in the very low energy region, which can easily escape one's notice.

The unsymmetrical species $[O_2{-}S_2]^+$ has its optical excitation energy higher than those for the symmetrical analogues because of the internal energy difference (ΔG°). Earlier work suggests that the ΔG° values for unsymmetrical complexes may also be estimated from the optical excitation energies for the structurally related symmetrical analogues.[18] In the present case, such an energetic correlation exists between $[O_2{-}S_2]^+$ and $[O_2{-}O_2]^+$ as indicated by eq 4:

$$\Delta G^\circ = \Delta E_{IT} = E_{IT}([O_2{-}S_2]^+) - E_{IT}([O_2{-}O_2]^+) \quad (4)$$

According to the spectroscopic data for $[O_2{-}S_2]^+$ (6560 cm^{-1}) and $[O_2{-}O_2]^+$ (4240 cm^{-1}), the internal energy difference ΔG° for $[O_2{-}S_2]^+$ is determined to be 2320 cm^{-1}. It is remarkable that the results from the spectroscopic and electrochemical methods are equal within experimental error. Thus, by the three different approaches, a ΔG° value of 2250 ± 80 cm^{-1} for $[O_2{-}S_2]^+$ is confirmed. Subtracting ΔG° (2320 cm^{-1}) from E_{IT} (6560 cm^{-1}) gives a total reorganization energy (λ) of 4240 cm^{-1} for the unsymmetrical analogue. It has shown that $[O_2{-}S_2]^+$ and $[O_2{-}O_2]^+$ have small and similar potential displacements ($\Delta E_{1/2}$), 84 and 91 mV, respectively. Consistently, these two complexes have large and equal reorganization energy (λ).

The electronic coupling matrix elements (H_{ab}) are calculated from the widely accepted Mulliken–Hush expression (eq 5):[11]

dx.doi.org/10.1021/ic4017855 | Inorg. Chem. 2013, 52, 12624–12633

$$H_{ab} = 2.06 \times 10^{-2} \frac{(\Delta\nu_{1/2}\varepsilon_{max}E_{IT})^{1/2}}{r_{ab}} \quad (5)$$

Here, the electron transfer distance (r_{ab}) is critical for accurate evaluation of the electronic coupling. Geometric distances between the bridged metal centers are usually used as the ET distances. However, it is realized that the coupling effect could be significantly underestimated because the effective ET distances (r'_{ab}) are shorter than the metal−metal separation.[14,25] As discussed earlier, for this Mo_2−Mo_2 series, the effective ET distance is estimated to be 5.8 Å from the geometrical length of the "$-CC_6H_4C-$" group. The obtained H_{ab} values increase constantly as the bridging ligand is stepwise thiolated (Table 5). This result is in good agreement with the electrochemical and spectroscopic analyses. The magnitude of H_{ab} is also comparable with the parameters found for the Ru−Ru compounds with similar metal to metal distance. For example, the H_{ab} value of 870 cm^{-1} for $[\mathbf{S_2}-\mathbf{S_2}]^+$ is close to 900 cm^{-1} for $[(NH_3)_5Ru)]_2$(4,4′-bpy), the electronic coupling corrected with the dipole moment change.[14b] When the $Mo_2\cdots Mo_2$ separation (ca. 11.8 Å) is used for the calculation, the H_{ab} value is 410 cm^{-1}, close to the reported value (446 cm^{-1}) for the 2,5-dihydoxylterephthalate bridged dimolybdenum pair based on r_{ab} = 11.3 Å.[26]Again, the H_{ab} values based on the metal−metal separations could be significantly underestimated. Since the Hush equation is only suitable for symmetrical compounds, there is no data derived for $[\mathbf{O_2}-\mathbf{S_2}]^+$.

Classification of the Mixed-Valence Compounds. Properly determining the classes of the mixed-valence complexes in terms of Robin−Day's scheme is another major issue. A quantitative criterion for classification of MV compounds is to examine the IT bandwidth using the following equation[24a]

$$\Gamma = 1 - (\Delta\nu_{1/2})/(2310\nu_{max})^{1/2} \quad (6)$$

In this expression, $\Delta\nu_{1/2}$ is the measured half-height bandwidth, while $(2310\nu_{max})^{1/2}$ is the predicted value for those in Class II. Compounds with the measured $\Delta\nu_{1/2}$ larger than the calculated value are generally considered to be in Class II. Both $[\mathbf{O_2}-\mathbf{O_2}]^+$ and $[\mathbf{OS}-\mathbf{OS}]^+$ present a negative Γ, ca. −0.17 and −0.14, respectively, and, thus, can be unambiguously assigned to the weakly coupled MV category or Class II. For $[\mathbf{S_2}-\mathbf{S_2}]^+$, on the other hand, the low energy, high intensity, as well as asymmetry of the IT band are unique. The near "half Gaussian" shaped band, as shown in Figure 6, provides direct evidence for the moderately strong metal to metal interaction (Figure 6 and Table 5). Figure 6 shows that the cutoff takes place at ~$2H_{ab}$ at the low energy side of the band. It is anticipated that a fully delocalized Class III species should have an optical transition energy $\lambda = 2H_{ab}$, which conforms well to the established theoretical framework.[24b,27] For $\lambda \sim 8000$ cm^{-1}, $\Gamma \approx 0.5$ is considered a criterion for the borderline between Class II and III systems. For systems with low energy intervalence transition, this Γ criterion should be less than 0.5.[24a] For example, although Ru−Ru complexes usually present high energy IT bands, a low energy and weak band (E_{IT}, 2000 cm^{-1} and ε_{IT}, 300 M^{-1} cm^{-1}) was found for Creutz−Taube ion.[28] Analyses on this mid-IR absorption band (Γ = 0.34) led to the conclusion that on the vibrational time scale the odd electron is fully delocalized. For $[\mathbf{S_2}-\mathbf{S_2}]^+$, the Γ value is increased to 0.30, while the intervalence transition is shifted to the mid-IR region. Given λ = 2640 cm^{-1} and $1 > 2H_{ab}/\lambda$ (0.65) > $[1-(4RT/\lambda)^{1/2}]$ (0.44),[24a,27] the fully thiolated $[\mathbf{S_2}-\mathbf{S_2}]^+$ is considered in the Class II−Class III transition regime, namely, "almost delocalized".[24c] Therefore, analyses on the IT bands indicate that the current system is approaching, but has not yet reached the Class III regime.

Prior to this work, Class II−III transitions were realized by changing the metal nuclearity into those having extended d orbitals, for example, from Ru to Os in d^{5-6} metal systems,[29] and Mo to W in M_2−M_2 systems.[26] In addition, an abrupt increase of the electronic coupling (H_{ab}) is observed as the systems cross the Class II−III regime. For example, the magnitudes of H_{ab} vary from 500 to 3240 cm^{-1} as the Class II−III transition occurs in organic radical systems.[4] It is notable that, in this study, the Class II−III transition takes place in the systems with $2H_{ab} \ll \lambda$, which is generally regarded as being weakly coupled. Therefore, it is evidenced that electronic coupling, as measured by H_{ab}, is not solely responsible for the electronic delocalization. Orbital interaction is another major factor that affects the charge distribution. For $[\mathbf{S_2}-\mathbf{S_2}]^+$, the strong metal−metal interaction should be attributed to the d(δ)−p(π) conjugation between the dimetal unit and the bridging ligand.

CONCLUSION

Convergent assembling of the dimetal precursor $Mo_2(DAniF)_3(O_2CCH_3)$ with a series of preprogrammed bridging ligands $(E_2CC_6H_4CE_2)^{2-}$ (E = O or S) has generated three symmetrical and one unsymmetrical dimolybdenum dimers, denoted as $[\mathbf{O_2}-\mathbf{O_2}]$, $[\mathbf{OS}-\mathbf{OS}]$, $[\mathbf{S_2}-\mathbf{S_2}]$, and $[\mathbf{O_2}$-$\mathbf{S_2}]$. While these compounds have similar molecular skeletons, the donor atoms on the bridging ligands are alternated with oxygen and sulfur. It is found that introducing sulfur donors onto the electron transfer platform improves greatly the electronic communication. For $[\mathbf{O_2}-\mathbf{S_2}]$, there exists an internal energy difference (ΔG°) of 2250 ± 80 cm^{-1} between the two dimetal sites, as determined by electrochemical and spectroscopic methods. DFT calculations yield the unbalanced molecular orbitals for the unsymmetrical compound, thus providing confirmation and interpretation to the experimental results.

The mixed-valence cation radicals $[\mathbf{O_2}-\mathbf{O_2}]^+$, $[\mathbf{OS}-\mathbf{OS}]^+$, $[\mathbf{S_2}-\mathbf{S_2}]^+$, and $[\mathbf{O_2}-\mathbf{S_2}]^+$ exhibit a g value of 1.942−1.947 in the EPR spectra, indicating that the odd electron resides essentially on a metal-based (δ) orbital. In considering that the δ electrons are delocalized over the $[Mo_2]$ coordination shell, the length of the central group "$-CC_6H_4C-$" (ca. 5.8 Å), rather than the geometrical distance between the two dimetal centers, is taken for the first time as the effective electron transfer distance in calculation of the electronic coupling constants (H_{ab}) from Mulliken−Hush equation. The obtained H_{ab} values fall in the range 600−900 cm^{-1}, which are very compatible with the results from electrochemical and spectroscopic analyses. By Robin−Day's scheme, while $[\mathbf{O_2}-\mathbf{O_2}]^+$ and $[\mathbf{OS}-\mathbf{OS}]^+$ belong to Class II, $[\mathbf{S_2}-\mathbf{S_2}]^+$ is situated on the borderline between Class II and III. Such a transition from localized to "almost delocalized" behaviors is seldom seen, especially in systems with $2H_{ab} \ll \lambda$ and large metal to metal separation (12 Å). It is unusual that the two dimetal sites in $[\mathbf{S_2}-\mathbf{S_2}]^+$ are weakly coupled, as judged by the H_{ab} value, but strongly interacting, as indicated by the low energy and intense intervalence transition. These results reveal that, in addition to electronic coupling, orbital interaction is one of the major factors that govern the metal−metal interaction.

dx.doi.org/10.1021/ic4017855 | Inorg. Chem. 2013, 52, 12624−12633

EXPERIMENTAL SECTION

Materials and Methods. All manipulations were performed in a nitrogen-filled glovebox or by using standard Schlenk-line techniques. All solvents were purified using a Vacuum Atmosphere (VAC) solvent purification system or freshly distilled over appropriate drying agents under nitrogen. Ligand and complexes, HDAniF,[13] $Mo_2(DAniF)_3(O_2CCH_3)$,[15a] and $[Mo_2(DAniF)_3](\mu\text{-}S_2CC_6H_4CS_2)$,[16] were synthesized according to published methods.

Physical Measurements. Elemental analyses were determined using an Elementar Vario EL elemental analyzer. UV−vis and NIR spectra were measured on a Shimadzu UV-3600 UV−vis−NIR spectrophotometer. The mid-infrared spectra were recorded on a Thermo Electron Corporation Nicolet 6700 spectrophotometer. Both near-IR and IR spectra were measured in CH_2Cl_2 solutions using IR quartz cells with light path length of 1 cm. Cyclic voltammograms (CVs) were performed using a CH Instruments model-CHI660D electrochemical analyzer in 0.10 M $^nBu_4NPF_6$ solution in CH_2Cl_2 with Pt working and auxiliary electrodes, Ag/AgCl reference electrode, and a scan rate of 100 mV/s. All potentials are referenced to the Ag/AgCl electrode. ^{1}H NMR spectra were recorded on a Bruker-400 spectrometer. EPR spectra were measured using a Bruker A300-10-12 electron paramagnetic resonance spectrometer. Measurements for the mixed-valence complexes were carried out in situ after single electron oxidation of the corresponding neutral compounds.

X-ray Structure Determinations. Single-crystal data for [**OS**−**OS**]·$4.5CH_2Cl_2$ and [$\mathbf{O_2}$−$\mathbf{S_2}$]·$5CH_2Cl_2$ were collected at 150 K on an Oxford Gemini S Ultra diffractometer with Cu Kα radiation (λ = 1.541 78 Å), and the empirical absorption corrections were applied using spherical harmonics, implemented in the SCALE3 ABSPACK scaling algorithm.[30] Single-crystal data for [$\mathbf{S_2}$−$\mathbf{S_2}$]·$2.6CH_2Cl_2$·$1.5CH_3CH_2OH$ were collected at 173(2) K on a Bruker SMART 1000 CCD area detector system with Mo Kα radiation (λ = 0.710 73 Å), and absorption corrections were performed using the SADABS program.[31] All the structures were solved using direct methods, which yielded the positions of all non-hydrogen atoms. Hydrogen atoms were placed in calculated positions in the final structure refinement. Structure determination and refinement were carried out using the SHELXS-97 and SHELXL-97 programs, respectively.[32] All non-hydrogen atoms were refined with anisotropic displacement parameters.

Computational Details. All DFT (density functional theory) calculations were performed with the hybrid O3LYP[33] functional implemented in the Gaussian 09 package (Revision A0.2).[34] The model complexes are fully optimized. The standard 6-31G* basis set was used for H, C, N atoms, and aug-CC-pvDZ basis set for S and O atoms of the bridging ligands. The SDD basis set together with SDD pseudopotential were used for the heavy metal Mo atoms. Time-dependent DFT (TD-DFT) calculations were carried out to obtain 60 excitations for all the model compounds. By replacing the *p*-anisyl groups on $[Mo_2(DAniF)_3]^+$ with hydrogen atoms, the employed calculation models have $[Mo_2(NHCHNH)_3]^+$ units as the building blocks. This simplification has been successfully used in the Mo_2 analogues.[8c,35]

Preparation of $[Mo_2(DAniF)_3]_2(\mu\text{-}O_2CC_6H_4CS_2)$. $Mo_2(DAniF)_3(O_2CCH_3)$ (0.103 g, 0.10 mmol) and piperidinium 4-dithiocarboxylatobenzoate (0.019 g, 0.05 mmol) were mixed in 30 mL of THF in a 100-mL flask. After the solution was vigorously stirred for 2 h at room temperature, a green-blue solid formed. The solvents were removed under vacuum. The residue was loaded on a neutral Al_2O_3 column and eluted with dichloromethane/hexane (15:1, v/v). Pure product was obtained by collecting the blue-green band. Yield: 0.0763 g (72%). Diffusion of ethanol into a dichloromethane solution of the compound affords green needle crystals. ^{1}H NMR δ (ppm in $CDCl_3$): 8.53 (s, 1H, −NC*H*N−), 8.51 (s, 1H, −NC*H*N−), 8.38 (d, 2H, aromatic C−*H*), 8.37 (s, 2H, −NC*H*N−), 8.31 (s, 2H, −NC*H*N−), 8.30 (d, 2H, aromatic C−*H*), 6.58 (m, 32H, aromatic C−*H*), 6.48 (d, 4H, aromatic C−*H*), 6.45 (d, 4H, aromatic C−*H*), 6.27 (d, 4H, aromatic C−*H*), 6.13 (d, 4H, aromatic C−*H*), 3.74 (s, 24H, −OCH_3), 3.67 (s, 12H, −OCH_3). UV−vis, λ_{max} nm (ε, M^{-1} cm^{-1}): 637 (2.3×10^4). Anal. Calcd for $C_{98}H_{94}Mo_4N_{12}O_{14}S_2$: C, 55.74; H, 4.49; N, 7.96; S, 3.04. Found: C, 55.25; H, 4.56; N, 7.68; S, 2.87.

Preparation of $[Mo_2(DAniF)_3]_2(\mu\text{-}SOCC_6H_4COS)$. A 100-mL Schlenk flask was charged with dithioterephthalic acid (0.050 g, 0.25 mmol) and $Mo_2(DAniF)_3(O_2CCH_3)$ (0.500 g, 0.50 mmol), to which 20 mL of THF was added. Upon mixing, a dark-blue solution was produced. The solution was stirred at room temperacture for 4 h. The solvent was evaporated under reduced pressure. The dark-blue residue was washed with ethanol (3 × 20 mL) and then dried under vacuum. Yield: 0.41 g (80%). Green needle crystals were obtained by diffusion of ethanol into a dichloromethane solution of the compound. ^{1}H NMR δ (ppm in $CDCl_3$): 8.52 (s, 2H, −NC*H*N−), 8.35 (s, 4H, −NC*H*N−), 8.27 (s, 4H, aromatic C−*H*), 6.67 (d, 16H, aromatic C−*H*), 6.53 (d, 16H, aromatic C−*H*), 6.44 (d, 8H, aromatic C−*H*), 6.22 (d, 8H, aromatic C−*H*), 3.74 (s, 24H, −OCH_3), 3.69 (s, 12H, −OCH_3). UV−vis, λ_{max} nm (ε, M^{-1} cm^{-1}): 460 (5.4×10^3), 618 (2.6×10^4). Anal. Calcd for $C_{98}H_{94}Mo_4N_{12}O_{14}S_2$: C, 55.74; H, 4.49; N, 7.96; S, 3.04. Found: C, 55.08; H, 4.45; N, 7.76; S, 3.16.

Preparation of $[Mo_2(DAniF)_3]_2(\mu\text{-}O_2CC_6H_4CO_2)$. The procedure described here is different from that reported earlier.[13] A solution of sodium ethoxide (0.014 g, 0.20 mmol) in 10 mL of ethanol was transferred to a solution of $Mo_2(DAniF)_3(O_2CCH_3)$ (0.203 g, 0.20 mmol) in 20 mL of THF. The solution was stirred at room temperature for 2 h before the solvents were removed under vacuum. The residue was dissolved using 25 mL of CH_2Cl_2 and filtered off through a Celite-packed funnel. The filtrate was mixed with tetraethylammonium terephthalate (0.0212 g, 0.05 mmol) in 10 mL of ethanol. The mixture was stirred for 3 h, producing a purple-red microcrystalline solid. The product was collected by filtration and washed with ethanol (3 × 20 mL). Yield: 0.148 g (71%). ^{1}H NMR δ (ppm in $CDCl_3$): 8.52 (s, 2H, −NC*H*N−), 8.38 (s, 4H, −NC*H*N−), 8.37 (s, 4H, aromatic C−*H*), 6.66 (d, 16H, aromatic C−*H*), 6.60 (d, 16H, aromatic C−*H*), 6.48 (d, 8H, aromatic C−*H*), 6.29 (d, 8H, aromatic C−*H*), 3.74 (s, 24H, −OCH_3), 3.70 (s, 12H, −OCH_3). UV−vis, λ_{max} nm (ε, M^{-1} cm^{-1}): 490 (1.5×10^4). Anal. Calcd for $C_{100}H_{98}Mo_4N_{12}O_{16}$: C, 56.99; H, 4.69; N, 7.97. Found: C, 56.67; H, 4.77; N, 7.97.

ASSOCIATED CONTENT

Supporting Information

Core structures, ^{1}H NMR data, cyclic voltammetry and differential pulse voltammetry data for $Mo_2(DAniF)_3(O_2CC_6H_5)$ and $Mo_2(DAniF)_3(S_2CC_6H_5)$, UV−vis data. Spectra predicted at TD-O3LYP theory level and simulated with Swizard software. Crystallographic data in CIF format. This material is available free of charge via the Internet at http://pubs.acs.org.

AUTHOR INFORMATION

Corresponding Author

*E-mail: tcyliu@jnu.edu.cn (C.Y.L.).

Notes

The authors declare no competing financial interest.

ACKNOWLEDGMENTS

We thank the National Natural Science Foundation of China (20871093, 90922010), Tongji University, Jinan University, and Sun Yat-Sen University for financial support.

REFERENCES

(1) (a) Creutz, C.; Taube, H. *J. Am. Chem. Soc.* **1969**, *91*, 3988−3989. (b) Creutz, C.; Taube, H. *J. Am. Chem. Soc.* **1973**, *95*, 1086−1094.

(2) (a) Creutz, C. *Prog. Inorg. Chem.* **1983**, *30*, 1−73. (b) Crutchley, R. J. *Adv. Inorg. Chem.* **1994**, *41*, 273−325. (c) Richardson, D. E.;

Taube, H. *Coord. Chem. Rev.* **1984**, *60*, 107−129. (d) Kaim, W.; Lahiri, G. K. *Angew. Chem., Int. Ed.* **2007**, *46*, 1778−1796.
(3) (a) Ito, T.; Hamaguchi, T.; Nagino, H.; Yamaguchi, T.; Washington, J.; Kubiak, C. P. *Science* **1997**, *277*, 660−663. (b) Ito, T.; Hamaguchi, T.; Nagino, H.; Yamaguchi, T.; Kido, H.; Zavarine, I. S.; Richmond, T.; Washington, J.; Kubiak, C. P. *J. Am. Chem. Soc.* **1999**, *121*, 4625−4632. (c) Ito, T.; Imai, N.; Yamaguchi, T.; Hamaguchi, T.; Londergan, C. H.; Kubiak, C. P. *Angew. Chem., Int. Ed.* **2004**, *43*, 1376−1381. (d) Salsman, J. C.; Kubiak, C. P. *J. Am. Chem. Soc.* **2005**, *127*, 2382−2383.
(4) Lambert, C.; Nöll, G. *J. Am. Chem. Soc.* **1999**, *121*, 8434−8442.
(5) Nelsen, S. F.; Ismagilov, R. F.; Trieber, D. A., II. *Science* **1997**, *278*, 846−849.
(6) Heckmann, A.; Lambert, C. *Angew. Chem., Int. Ed.* **2012**, *51*, 326−392.
(7) (a) Cayton, R. H.; Chisholm, M. H.; Huffman, J. C.; Lobkovsky, E. B. *J. Am. Chem. Soc.* **1991**, *113*, 8709−8724. (b) Cayton, R. H.; Chisholm, M. H.; Huffman, J. C.; Lobkovsky, E. B. *Angew. Chem., Int. Ed.* **1991**, *30*, 862−864.
(8) (a) Cotton, F. A.; Lin, C.; Murillo, C. A. *J. Chem. Soc., Dalton Trans.* **1998**, 3151−3153. (b) Cotton, F. A.; Donahue, J. P.; Murillo, C. A. *J. Am. Chem. Soc.* **2003**, *125*, 5436−5450. (c) Cotton, F. A.; Donahue, J. P.; Murillo, C. A.; Pérez, L. M. *J. Am. Chem. Soc.* **2003**, *125*, 5486−5492.
(9) Cotton, F. A.; Murillo, C. A.; Walton, R. A. *Multiple Bonds between Metal Atoms*, 3rd ed.; Springer: New York, 2005.
(10) (a) Cotton, F. A.; Donahue, J. P.; Lin, C.; Murillo, C. A.; Rockwell, J. *Acta Crystallogr.* **2002**, *E58*, m298−m300. (b) Cotton, F. A.; Donahue, J. P.; Lin, C.; Murillo, C. A. *Inorg. Chem.* **2001**, *40*, 1234−1244.
(11) (a) Hush, N. S. *Prog. Inorg. Chem.* **1967**, *8*, 391−444. (b) Hush, N. S. *Coord. Chem. Rev.* **1985**, *64*, 135−157.
(12) Robin, M. B.; Day, P. *Adv. Inorg. Chem. Radiochem.* **1967**, *10*, 247−422.
(13) Lin, C.; Protasiewicz, J. D.; Smith, E. T.; Ren, T. *Inorg. Chem.* **1996**, *35*, 6422−6428.
(14) (a) Karki, L.; Lu, H. P.; Hupp, J. T. *J. Phys. Chem.* **1996**, *100*, 15637−15639. (b) Brunschwig, B. S.; Creutz, C.; Sutin, N. *Coord. Chem. Rev.* **1998**, *177*, 61−79.
(15) (a) Cotton, F. A.; Liu, C. Y.; Murillo, C. A.; Villagrán, D.; Wang, X. *J. Am. Chem. Soc.* **2003**, *125*, 13564−13575. (b) Cotton, F. A.; Li, Z.; Liu, C. Y.; Murillo, C. A. *Inorg. Chem.* **2007**, *46*, 7840−7847.
(16) Han, M. J.; Liu, C. Y.; Tian, P. F. *Inorg. Chem.* **2009**, *48*, 6347−6349.
(17) (a) Marcus, R. A. *J. Chem. Phys.* **1965**, *43*, 679−701. (b) Marcus, R. A. *Angew. Chem., Int. Ed.* **1993**, *32*, 1111−1222. (c) Marcus, R. A.; Sutin, N. *Comments Inorg. Chem.* **1986**, *5*, 119−133.
(18) Goldsby, K. A.; Meyer, T. J. *Inorg. Chem.* **1984**, *23*, 3002−3010.
(19) Evans, C. E. B.; Naklicki, M. L.; Rezvani, A. R.; White, C. A.; Kondratiev, V. V.; Crutchley, R. J. *J. Am. Chem. Soc.* **1998**, *120*, 13096−13103.
(20) Richardson, D. E.; Taube, H. *Inorg. Chem.* **1981**, *20*, 1278−1285.
(21) Chisholm, M. H.; Patmore, N. J. *J. Chem. Soc., Dalton Trans.* **2006**, 3164−3169.
(22) Barybin, M. V.; Chisholm, M. H.; Dalal, N. S.; Holovics, T. H.; Patmore, N. J.; Robinson, R. E.; Zipse, D. J. *J. Am. Chem. Soc.* **2005**, *127*, 15182−15190.
(23) Cotton, F. A.; Liu, C. Y.; Murillo, C. A.; Zhao, Q. *Inorg. Chem.* **2007**, *46*, 2604−2611.
(24) (a) Brunschwig, B. S.; Creutz, C.; Sutin, N. *Chem. Soc. Rev.* **2002**, *31*, 168−184. (b) D'Alessandro, D. M.; Keene, F. R. *Chem. Soc. Rev.* **2006**, *35*, 424−440. (c) Nelsen, S. F. *Chem.—Eur. J.* **2000**, *6*, 581−588.
(25) Hupp, J. T.; Dong, Y.; Blackbourn, R. L.; Lu, H. *J. Phys. Chem.* **1993**, *97*, 3278−3282.
(26) Chisholm, M. H.; Feil, F.; Hadad, C. M.; Patmore, N. J. *J. Am. Chem. Soc.* **2005**, *127*, 18150−18158.
(27) Brunschwig, B. S.; Sutin, N. *Coord. Chem. Rev.* **1999**, *187*, 233−254.
(28) Best, S. P.; Clark, R. J. H.; McQueen, R. C. S.; Joss, S. *J. Am. Chem. Soc.* **1989**, *111*, 548−550.
(29) Demadis, K. D.; Neyhart, G. A.; Kober, E. M.; Meyer, T. J. *J. Am. Chem. Soc.* **1998**, *120*, 7121−7122.
(30) *CrysAlis RED, Version 1.171.31.7*; Oxford Diffraction Ltd.: Abington, U.K., 2006.
(31) Sheldrick, G. M. *SADABS, Program for Empirical Absorption Correction of Area Detector Data*; University of Göttingen: Göttingen, Germany, 1996.
(32) Sheldrick, G. M. *SHELXTL, Version 6.12*; Bruker Analytical X-ray Systems, Inc.: Madison, WI, 2000.
(33) (a) Cohen, A. J.; Handy, N. C. *Mol. Phys.* **2001**, *99*, 607−615. (b) Lee, C.; Yang, W.; Parr, R. G. *Phys. Rev. B* **1988**, *37*, 785−789.
(34) Frisch, M. J.; Trucks, G. W.; Schlegel, H. B.; Scuseria, G. E.; Robb, M. A.; Cheeseman, J. R.; Scalmani, G.; Barone, V.; Mennucci, B.; Petersson, G. A.; Nakatsuji, H.; Caricato, M.; Li, X.; Hratchian, H. P.; Izmaylov, A. F.; Bloino, J.; Zheng, G.; Sonnenberg, J. L.; Hada, M.; Ehara, M.; Toyota, K.; Fukuda, R.; Hasegawa, J.; Ishida, M.; Nakajima, T.; Honda, Y.; Kitao, O.; Nakai, H.; Vreven, T.; Montgomery, J. A., Jr.; Peralta, J. E.; Ogliaro, F.; Bearpark, M.; Heyd, J. J.; Brothers, E.; Kudin, K. N.; Staroverov, V. N.; Kobayashi, R.; Normand, J.; Raghavachari, K.; Rendell, A.; Burant, J. C.; Iyengar, S. S.; Tomasi, J.; Cossi, M.; Rega, N.; Millam, J. M.; Klene, M.; Knox, J. E.; Cross, J. B.; Bakken, V.; Adamo, C.; Jaramillo, J.; Gomperts, R.; Stratmann, R. E.; Yazyev, O.; Austin, A. J.; Cammi, R.; Pomelli, C.; Ochterski, J. W.; Martin, R. L.; Morokuma, K.; Zakrzewski, V. G.; Voth, G. A.; Salvador, P.; Dannenberg, J. J.; Dapprich, S.; Daniels, A. D.; Farkas, O.; Foresman, J. B.; Ortiz, J. V.; Cioslowski, J.; Fox, D. J. *Gaussian 09, Revision A0.2*; Gaussian, Inc.: Wallingford, CT, 2009.
(35) Cotton, F. A.; Liu, C. Y.; Murillo, C. A.; Villagrán, D.; Wang, X. *J. Am. Chem. Soc.* **2004**, *126*, 14822−14831.